



# Modification of C/TiO<sub>2</sub>@MCM-41 with nickel nanoparticles for photocatalytic desulfurization enhancement of a diesel fuel model under visible light

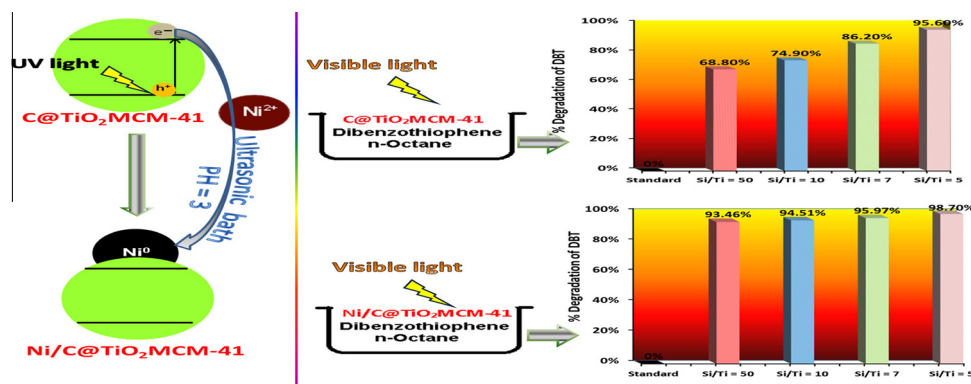


M. Zarrabi<sup>a</sup>, M.H. Entezari<sup>a,b,\*</sup>

<sup>a</sup>Sonochemical Research Center, Department of Chemistry, Faculty of Science, Ferdowsi University of Mashhad, 91779 Mashhad, Iran

<sup>b</sup>Environmental Chemistry Research Center, Department of Chemistry, Faculty of Science, Ferdowsi University of Mashhad, 91779 Mashhad, Iran

## GRAPHICAL ABSTRACT



## ARTICLE INFO

### Article history:

Received 20 May 2015

Revised 9 July 2015

Accepted 10 July 2015

Available online 10 July 2015

### Keywords:

C/TiO<sub>2</sub>@MCM-41 (CTM-41)

Ni nanoparticles

Desulfurization

Dibenzothiophene (DBT)

Photocatalyst

Visible light

## ABSTRACT

Ni metal nanoparticles were attached on the C/TiO<sub>2</sub>@MCM-41 (CTM-41) via facile and fast method based on dispersing of C/TiO<sub>2</sub>@MCM-41 in aqueous solution containing nickel ions by ultrasonic bath. Then, for the first time, the Ni ions were converted to Ni nanoparticles under UV light (photo-assisted deposition, PAD method), without using reducing agents and hydrogen gas. This process was carried out under the relatively mild conditions. The results showed that Ni (II) was reduced to Ni metallic nanoparticle in the size of about 2.7 nm on the surface of CTM-41 (Ni/CTM-41) with specific surface area of 754.37 m<sup>2</sup> g<sup>-1</sup>. The photocatalytic ultra-deep desulfurization of a fuel-like n-octane containing dibenzothiophene (DBT) was conducted over the Ni/CTM-41 nanophotocatalyst. Using this method, the total sulfur content efficiently decreased under mild conditions in one phase and without using an oxidant. The synthesized Ni/CTM-41 (3% Ni) exhibited the maximum photocatalytic desulfurization of DBT for all different ratios of Si/Ti. In contrast, the synthesized CTM-41 (without Ni) exhibited the maximum photocatalytic desulfurization of DBT only for minimum ratio of Si/Ti. The Ni/CTM-41 was characterized by several techniques including N<sub>2</sub> adsorption-desorption isotherms, XRD, TEM, and atomic absorption spectroscopy techniques. The results confirmed that Ni was highly dispersed on the support phase. The GC-MS analysis confirmed the photocatalytic removal of DBT. Based on the experimental results, it is proposed that the hydroxyl radical and hole have key role in the photocatalytic desulfurization process.

© 2015 Elsevier Inc. All rights reserved.

\* Corresponding author at: Sonochemical Research Center, Environmental Chemistry Research Center, Department of Chemistry, Faculty of Science, Ferdowsi University of Mashhad, 91779 Mashhad, Iran.

E-mail addresses: [entezari@um.ac.ir](mailto:entezari@um.ac.ir), [moh\\_entezari@yahoo.com](mailto:moh_entezari@yahoo.com) (M.H. Entezari).

## 1. Introduction

The reduction of sulfur content in commercial fuels (gasoline and diesel oil) is important for improving air quality because they are the main sources of SO<sub>x</sub> emissions, a major air pollutant [1–3]. Deep desulfurization of commercial fuels is significant not only for clean air but also for use in fuel cell. The sulfur concentration of the fuel needs to be ultra-low (<1 ppm). Hydrodesulfurization (HDS) is a conventional process for removing sulfur compounds such as thiols, sulfides, disulfides, thiophenes, and benzothiophene. This method is less effective for removing dibenzothiophene (DBT) and its derivatives. In conventional HDS, it is difficult to reduce the sulfur of liquid fuels to a very low level (<1 ppm). In order to reach sulfur level to zero, refractory sulfur compounds such as DBT and its derivatives must be separated from diesel fuels [4–7].

Oxidative desulfurization (ODS) is considered to be one of the promising new methods for deep desulfurization of fuel. This is due to the low cost of ODS and it can be carried out under very mild conditions. As a kind of ODS technique [8–10], the photocatalytic ODS is also an attracting method [2,11].

Several studies showed that the refractory compounds especially 4,6-dimethyl dibenzothiophene (4,6-DMDBT) bind tightly by an electronic back bonding between species adsorbed to the surface of an adsorbent through the formation of  $\pi$ -complexes. This usually occurs between a transition metal and the aromatic rings of the adsorbed species. In the  $\pi$ -complexation mechanism, the cation can form the usual  $\sigma$ -bonds with their *s*-orbitals while their *d*-orbitals can back-donate electron density to the antibonding  $\pi$ -orbitals of sulfur rings. The metals with  $nd^xns^0$  ( $x = 5-10$ ) electronic configuration can form a strong electronic bonding to achieve  $\pi$ -complexation. The metals also possess an empty *s* orbital, capable of accepting electron density, and the *d* orbitals with electrons available for back donation, for example Ni with a [Ar] 3d<sup>8</sup>4s<sup>0</sup> electronic configuration. However, to achieve an adsorption process these metals should have a suitable support [12–15].

Recently, we carried out ODS technique for photodesulfurization of DBT with CTM-41 [16]. The objective of the present study is to improve the desulfurization performance by deposition of Ni nanoparticles on CTM-41. Mesoporous molecular sieves (CTM-41) and ultrasonic bath were used to increase the nickel dispersion. In deposition process, the PAD method was employed and the pH was adjusted at the isoelectric point of photocatalysis.

## 2. Experimental

### 2.1. Materials

Tetrabutylortotitanate (98%), ethanol (99.5%), dimethyl sulfoxide (DMSO, 99%), ammonium oxalate (AO, 99.5%), nickel nitrate (Ni(NO<sub>3</sub>)<sub>2</sub>·6H<sub>2</sub>O), and hexane were supplied by Merck. DBT, tetrachloride titanate (TiCl<sub>4</sub>, 99.9%) and p-benzoquinone (BQ) from Sigma–Aldrich, *n*-octane (95%) from Samchun, and MCM-41 from Gas Chem Company of China. De-ionized water was used in the preparation of the catalyst.

### 2.2. Preparation of Ni/CTM-41 nanocomposites

CTM-41 nanocomposite was prepared according to our previous work [16]. The pH<sub>pzc</sub> of CTM-41 was determined at 3 by using the drift method [17]. A desired amount of degased Ni(NO<sub>3</sub>)<sub>2</sub>·6H<sub>2</sub>O solution (0.004 M) was slowly added into the suspension containing 0.15 g CTM-41 at room temperature. The mixture was stirred by a mechanical stirring under Ar gas atmosphere [18] and the pH of the suspension was adjusted to 2.9–3.0 by HCl aqueous solution (5 mM).

At pH = 3, the zeta potential of CTM-41 was zero, therefore, Ni ions cannot be adsorbed on the surface of CTM-41 which is helpful for the photoreduction of Ni<sup>2+</sup> to Ni<sup>0</sup> without going into nickel oxide. The mixture was kept in the ultrasonic bath for 1 h under Ar gas. Then, the system was stirred for 2 h at room temperature under argon gas to remove the air in the solution.

The suspension was photo irradiated by 300 W high pressure mercury lamp for 5 h. Then, the solid phase was separated from the mixture using centrifugation at rate of 5000 rpm. It was washed four times with deionized water and the product was dried in an oven at 100 °C overnight. The samples with Si/Ti ratios of 50, 10, 7 and 5 were named Ni/CTM-41 (50), Ni/CTM-41 (10), Ni/CTM-41 (7), Ni/CTM-41 (5), respectively.

### 2.3. Characterization techniques

The X-ray diffraction (XRD) was performed by Bruker-axs, D8 Advance model, with monochromatized Cu K $\alpha$  radiation ( $\lambda = 1.5406$  Å). Optical absorption spectra of the DBT were measured using UV–Vis spectroscopy (Unico 2800). The N<sub>2</sub> adsorption isotherms of samples were studied at 77 K on a Belgian apparatus (Belsorp mini II model). The isotherms were used to calculate BET specific surface areas, pore volumes, and pore sizes of the powder samples. The particle size of the deposited Ni metal was determined with transmission electron microscope (TEM, Philips CM-120). The GC–MS (Agilent-6890, MSD: 5973N) was used for determining the degradation products.

### 2.4. Photocatalytic degradation of DBT

The degradation was performed under constant stirring in a 50 mL glass vessel with a plug. As a model fuel, 10 mL of *n*-octane solution of DBT (300 ppm) was placed in a vessel and a specified amount of catalyst was added. Before illumination, the suspension was magnetically stirred to attain adsorption–desorption equilibrium between photocatalyst and DBT for 45 min in the dark and then it was illuminated with two 300 W tungsten lamps (visible irradiation) at 333 K for 5 h. External oxidative or radical-generating sources were not added to the mixture. The absorption of DBT was monitored with a UV–Vis spectrophotometer at  $\lambda_{\max} = 325$  nm [19]. The strong absorbance at 325 nm suggests a  $n \rightarrow \pi^*$  excitation similar to that for the sulfur atom in DBT. Then, the absorption was converted to the concentration through the standard curve. The degradation of DBT was calculated according to the initial, C<sub>0</sub> (mg/L) and final, C (mg/L) concentrations of DBT in the solution:

$$x = ((C - C_0)/C_0) \times 100$$

where *x* stands for the degradation percent. To prove of degradation of DBT, the liquid phase was separated from catalyst by centrifuge. Then, the organic phase and catalysis were extracted for GC–MASS analysis.

## 3. Results and discussion

### 3.1. Photodeposition of Ni precursor

In our previous work [16], the formation of an ordered mesoporous structure of CTM-41 was confirmed. It was also indicated the presence of anatase (isolated Ti-oxide moieties in CTM-41) and tetrahedrally coordinated Ti oxide moieties (Ti<sup>4+</sup>) within the framework of the CTM-41 [20–22].

As shown in Fig. 1, the UV–Vis spectra of CTM-41 (Si/Ti = 50) exhibited a very intense and narrow UV absorption at around 200–210 nm. Also, a peak shoulder is observed at 230 nm. Le Noc

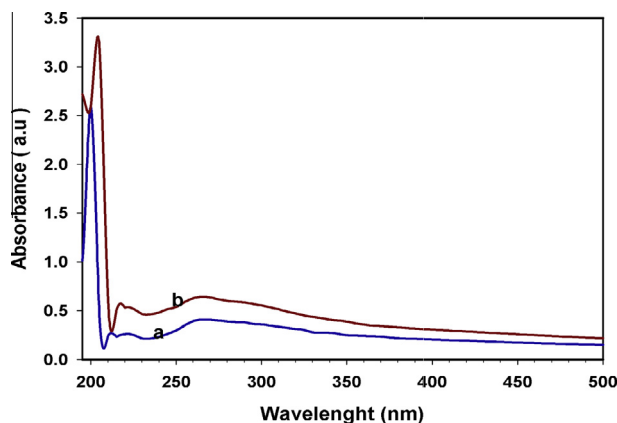
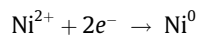
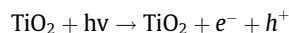


Fig. 1. UV-Visible spectra for: (a) CTM-41 (50) and (b) Ni/CTM-41 (50).

et al. suggested that the two bands at 200–210 and 230 nm are due to the two different framework sites  $[\text{Ti}(\text{OH})(\text{OSi})_3]$  and  $[\text{Ti}(\text{OSi})_4]$  which indicates that the titanium exists mainly in tetrahedral coordination. These two peaks arise from oxygen ligand to tetrahedral titanium-(IV) charge transfer (LMCT) as represented in Eq. (1) [23]:



The additional broad shoulder in the range of 250–350 nm indicates the presence of Ti–O–Ti connectivities and/or five or six-coordinated titanium species which can appear upon hydration by insertion of water molecules as extra ligands [24,25]. The Ni/CTM-41 samples have different absorption in UV-Vis spectra in comparison with CTM-41. This is due to the interactions between the Ni metallic nanoparticles and titania. The other UV-Vis spectra (see the Supporting Information, Figs. S 1–3) further confirm that the CTM-41 even with higher amount of  $\text{TiO}_2$  (Si/Ti = 10, 7, 5) show the framework described above. Under UV-light irradiation of Hg lamp with the wavelength < 400 nm, the CTM-41 could generate photo-excited electrons and positive holes [26]. The  $\text{Ni}^{2+}$  ion reduction takes place on the surface of  $\text{TiO}_2$  which has modified the surface of mesoporous MCM-41 in an aqueous  $\text{NiNO}_3$  solution. The Ni metal nanoparticles can be successfully deposited on the CTM-41.



Metallic nickel contents measured by atomic absorption spectroscopy in each of the samples are reported in Table 1. The exit of brown gas ( $\text{NO}_2$  gas) represents the reaction between nickel metal and concentrated nitric acid that confirmed the formation of metallic nickel.

Ni deposition was not observed neither on the mesoporous silica without Ti oxide under UV-light irradiation nor on the CTM-41 without UV-light irradiation. These results suggest that the Ni precursor underwent anchoring on the single framework  $\text{Ti}^{4+}$  center under UV-light.

Table 1  
Nickel loading amount on catalyst.

Ni	Sample
3.2	Ni/CTM-41 (50)
3.1	Ni/CTM-41 (10)
3.0	Ni/CTM-41 (7)
2.8	Ni/CTM-41 (5)

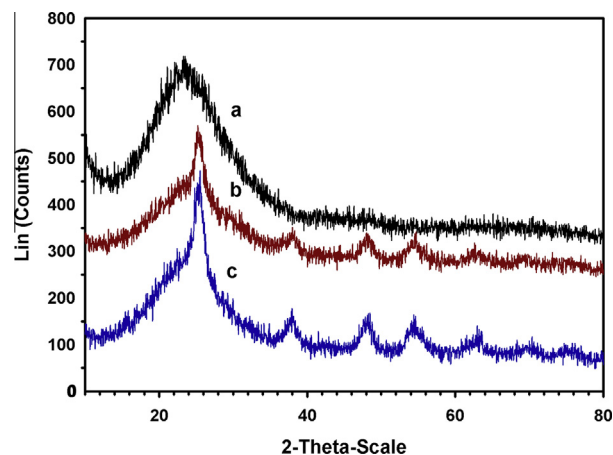


Fig. 2. XRD patterns of (a) MCM-41, (b) CTM-41(5) and (c) Ni/CTM-41(5).

X-ray diffraction patterns of MCM-41, CTM-41 (5) and Ni/CTM-41 (5) are illustrated in Fig. 2. The diffraction peaks appear at  $2\theta = 25.32^\circ, 37.99^\circ, 54.76^\circ, 48.05^\circ$  and  $62.68^\circ$  are typical patterns of anatase [27]. Fig. 2 shows the phase of both CTM-41 and Ni-CTM-41 is anatase phase. The loading of Ni does not affect on the crystallization performance of CTM-41. It is clear that the peak intensity of anatase increases [28] and the width of the diffraction peaks of anatase phase becomes narrower by loading Ni. This suggests that the particle size of anatase nanoparticles increases by loading Ni [29]. The average crystallite size of the sample was estimated using the Debye–Scherrer equation at  $2\theta = 25.32^\circ$  and  $46.36^\circ$ .

By increasing Ni loading, the crystallite sizes increase from 6.89 nm to 6.90 nm and from 5.66 nm to 7.84 nm for  $2\theta = 25.32^\circ$  and  $46.36^\circ$ , respectively. This might be attributed to the incorporation of Ni ion into the  $\text{TiO}_2$  lattice. Because the ionic radius of Ni ion (0.069 nm) is slightly larger than ionic radius of  $\text{Ti}^{4+}$  (0.068 nm), Ni could easily be incorporated into the  $\text{TiO}_2$  lattice, resulting in increasing the crystallite size of nanoparticles.

The  $\text{N}_2$  adsorption–desorption isotherms of Ni/CTM-41 (5), CTM-41(5) and MCM-41 samples were studied to assessment the mesoporous structures of samples (Fig. 3). When the relative pressure ( $p/p_0$ ) was between 0.3 and 0.4, a mark inflection was observed. This is caused by capillary condensation within the mesoporous structure. When the Ni was loaded, the inflection became weak. The specific surface area and pore volume decreased as can be seen from Table 2.

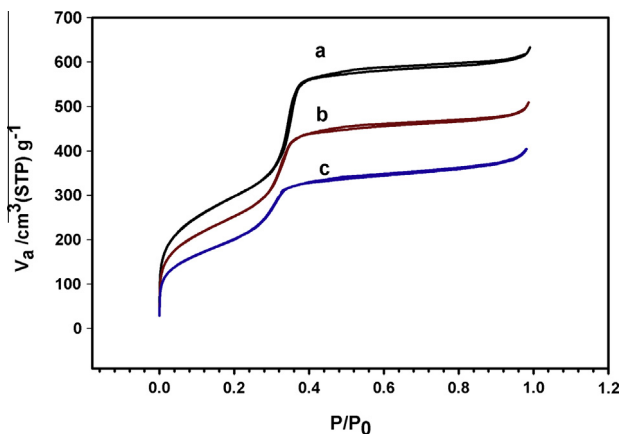


Fig. 3. Nitrogen adsorption–desorption isotherms of (a) MCM-41, (b) CTM-41 (5) and (c) Ni/CTM-41 (5).

**Table 2**  
Textural properties of MCM-41, CTM-41 (5) and Ni/CTM-41 (5).

	$D$ (nm)	$S_{\text{BET}}$ (m <sup>2</sup> /g)	$V$ (cm <sup>3</sup> /g)
MCM-41	3.63	1076.50	0.98
CTM-41(0.2)	3.42	922.42	0.79
Ni/CTM-41(0.2)	3.31	754.37	0.6251

$D$  (nm): average pore diameter,  $S_{\text{BET}}$  (m<sup>2</sup>/g): surface area,  $V$  (ml/g): pore volume.

The TEM images shown in Fig. 4 confirm the two-dimensional branched network structure of the synthesized Ni/CTM-41. The TEM images of Ni/CTM-41 indicate the Ni particles (dark field) are dispersed on the surface of CTM-41 support with mean particle size approximately 2.75 nm. Since the average pore size of Ni/CTM-41 (3.31 nm) is smaller than that of CTM-41 (3.42 nm) (see Table 2), some of the nickel particles should be positioned in the CTM-41 channels.

The UV–Vis absorption spectra in Fig. 1 and Figs. S 1–3 showed that the CTM-41 and Ni/CTM-41 are photoactive under visible light irradiation because these samples exhibit absorption bands from 400 to 800 nm.

Fig. 5 shows the band gap energy values of CTM-41 and Ni/CTM-41 with different Si/Ti ratios (50, 10, 7 and 5), that are calculated using Tauc's equation [30,31]. The calculated band gap energies are 1.3 and 3.2 eV.

According to our previous work [16], the band gaps of CTM-41 were assigned to the isolated C 2p states of carbonate ions and coke-like structure which have both been considered as the source of the extended optical absorption in the visible range. Since the band gaps of Ni/CTM-41 are similar to band gaps of CTM-41 at different ratios, it is suggested that Ni is dispersed on the surface of CTM-41.

### 3.2. Titania loading on desulfurization performance

In order to examine the effect of the loading amount of titania on desulfurization performance, four CTM-41 samples with different Si/Ti ratios (50, 10, 7 and 5) were prepared. Fig. 6 shows a comparison between desulfurization of solutions (DBT in *n*-octane) under dark and visible irradiation in the presence of CTM-41 with different Si/Ti ratios.

Desulfurization of DBT under dark proceeds via adsorption that it could be attributed to the mesoporosity of CTM-41 and Lewis acid sites of tetrahedral Ti species in the framework of the catalyst. As shown in Fig. 6, increasing Ti loading from Si/Ti = 50 to Si/Ti = 5 leads to an increase of desulfurization from 44.7% to 59.7% under dark condition. However, by increasing of Ti loading the total pore

volume of CTM-41 decreases (Table 2) but the Lewis acid sites of tetrahedral Ti species increase which is proper for the adsorption.

Desulfurization of DBT under visible light proceeds via degradation as it was showed in our previous work [16]. The photocatalytic activity of the samples with different ratios of Si to Ti was compared with each other. The catalyst synthesized with ratio of Si/Ti = 5 shows higher photocatalytic activity (95.6%) than that with ratio of Ti/Si = 50 (68.8%). Its higher activity may be attributed to the presence of more Ti in lowest ratio in CTM-41 (Si/Ti = 5).

### 3.3. Nickel loading on desulfurization performance

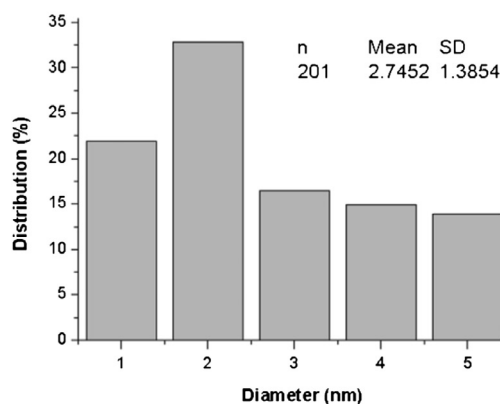
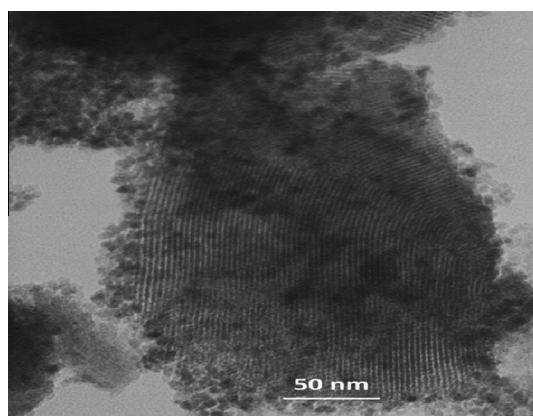
The catalytic performance of Ni/CTM-41 under dark and visible irradiation was investigated (Fig. 7). The desulfurization of DBT was higher with Ni/CTM-41 than that with CTM-41 in both under dark and light conditions.

Table 3 compares the desulfurization performance of Ni/CTM-41 and CTM-41 under visible light. This indicates that the nickel-based supports with different ratio of Si/Ti have stronger effect on the desulfurization performance. In another word, the degradation of dibenzothiophene under visible light from 68.6%, 74.9%, 86.2%, 95.6% for CTM-41 reaches to 93.5%, 94.5%, 96%, 98.6% for the nickel-based catalyst with ratios of Si/Ti = 50, 10, 7, and 5, respectively. Improving the photocatalytic degradation can be attributed to metal nickel that can help the charge separation and act as a co-catalyst for photocatalytic activity.

Also, Table 3 shows that the best dibenzothiophene removal percent is 59.7% for CTM-41 (Si/Ti = 5) in dark that can reach to 83.15% for Ni/CTM-41 (Si/Ti = 5). As a result, the desulfurization performance of Ni/CTM-41 was improved. The enhancement can be explained based on the Ni loading atoms which preferentially form a charge-transfer complex with benzene rings of DBT ( $\pi$ -complexation). Thus, the interaction between the substrate (Ni/CTM-41) and DBT increases and then the photocatalytic performance of Ni/CTM-41 under visible light can be increased too.

To clarify the mechanism of desulfurization of DBT, the experiments were performed using different radical scavengers in the presence of Ni/CTM-41 (Si/Ti = 50). Dimethyl sulfoxid (DMSO), ammonium oxalate (AO), *p*-benzoquinone (BQ) were used as scavengers of hydroxyl radicals ( $\text{OH}^\cdot$ ), holes ( $h^+$ ) and superoxide anion radicals ( $\text{O}_2^{\cdot-}$ ), respectively [32,33].

As it is shown in Fig. 8, when DMSO was added, desulfurization of DBT was remarkably inhibited. Addition of AO reduced desulfurization from 98.60% to 60.10%. Therefore, the hydroxyl radicals ( $\text{OH}^\cdot$ ) and hole are the primary oxidant in photocatalytic oxidation. When BQ as scavenger was used, desulfurization of DBT was reduced to about 20%. This implies that the superoxide anion



**Fig. 4.** TEM micrograph of Ni/CTM-41 (5) (left) and size distribution of Ni on the surface (right).

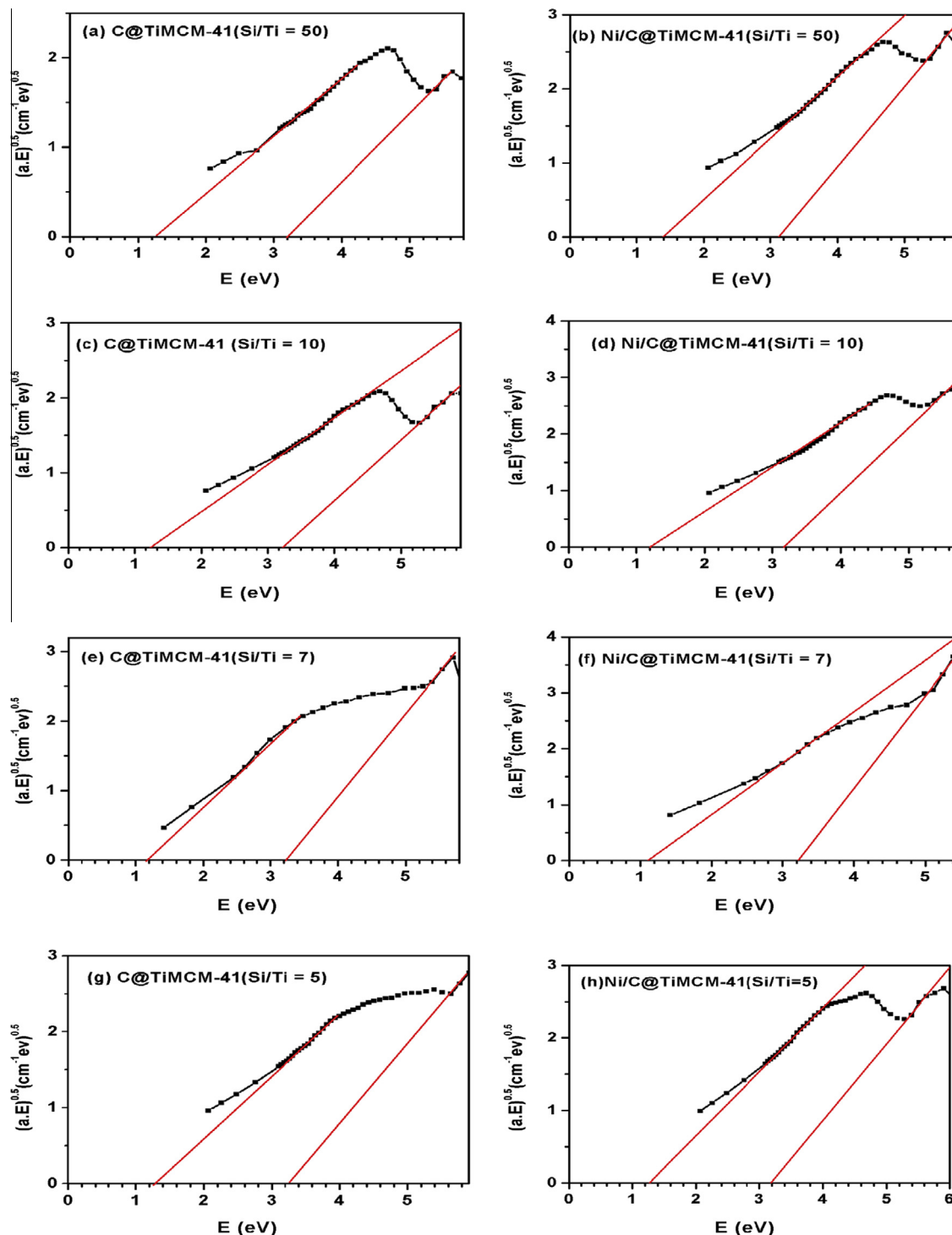
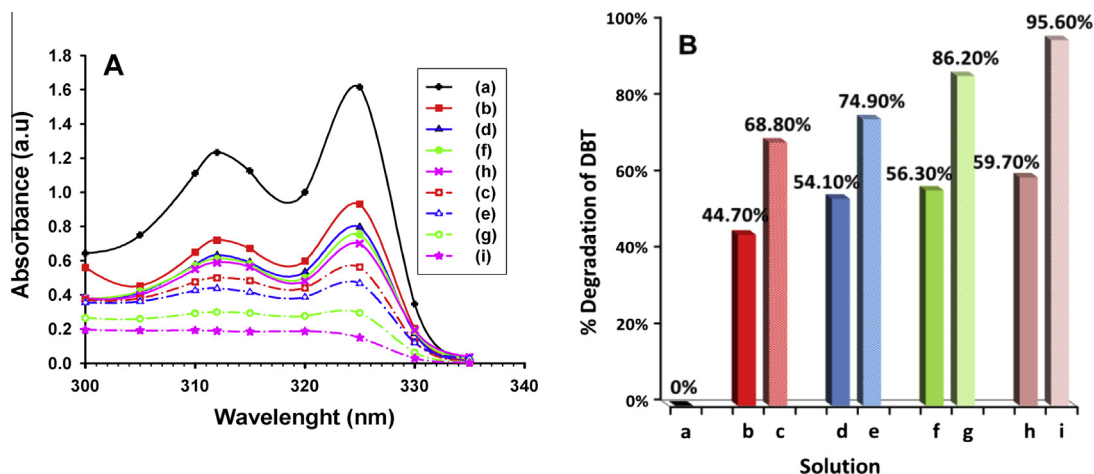


Fig. 5. Tauc's plots for Ni/CTM-41 and CTM-41 with different ratios.

radicals ( $O_2^{\cdot-}$ ) plays a minor role with respect to hydroxyl and hole in the degradation of DBT. Also, the usage of inert  $N_2$ -saturated atmosphere causes a small change in the desulfurization. This suggests that oxygen is not the primary oxidant in our photocatalytic oxidation system.

The behaviors of scavengers in the presence of Ni/CTM-41 are similar to the presence of CTM-41. This proved that the photocatalytic desulfurization of DBT by Ni/CTM41 done via direct reactions of DBT with oxidative species on the surface, similar to mechanism of the photocatalytic desulfurization of DBT by CTM-41. Addition

of Ni facilitates the degradation and a proposed mechanism for DBT degradation is presented in Fig. 9. In order to describe the photodegradation, the GC-MS analysis was used. The GC chromatogram for DBT solution (300 ppm) before photocatalytic degradation showed a peak at retention time ( $t_r$ ) of 34.78 min. This peak was identified by GC-MS analysis and compared with standard samples. The retention time was corresponded to DBT. After photocatalytic degradation and catalyst separation by centrifuging, a sulfur compound was not detected in the solution. To examine the adsorption of sulfur compounds on the surface, the



**Fig. 6.** (A) UV-Vis absorption spectra, (B) percentage of DBT degradation of DBT solution in presence of CTM-41 with different Si/Ti ( $x$ ) ratios: (b)  $x = 50$ , under dark (c)  $x = 50$ , under visible light, (d)  $x = 10$ , under dark, (e)  $x = 10$ , under visible light, (f)  $x = 7$ , under dark, (g)  $x = 7$ , under visible light, (h)  $x = 5$ , under dark and (i)  $x = 5$ , under visible light.

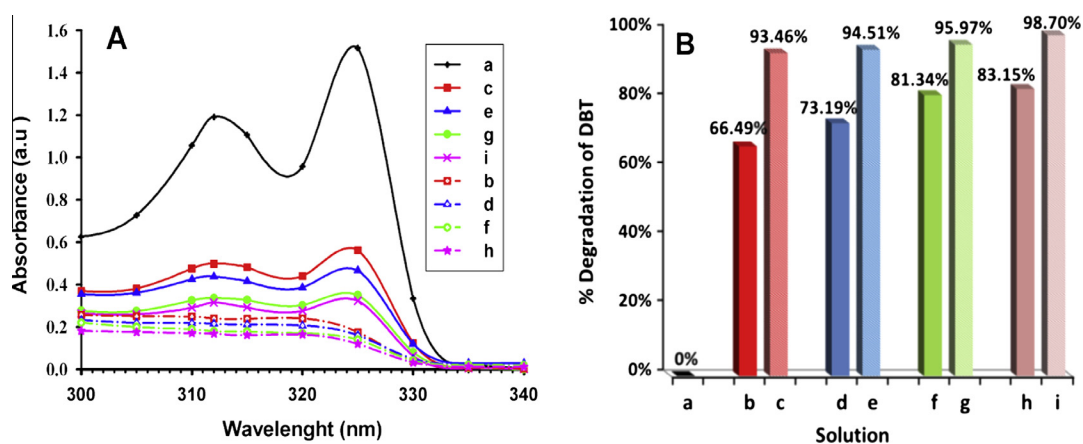


**Fig. 7.** (A) UV-Vis absorption spectra, (B) Percentage of DBT degradation of DBT solution in presence of Ni/CTM-41 with different Si/Ti ( $x$ ) ratios: (b)  $x = 50$ , under dark, (c)  $x = 50$ , under visible light, (d)  $x = 10$ , under dark, (e)  $x = 10$ , under visible light, (f)  $x = 7$ , under dark, (g)  $x = 7$ , under visible light, (h)  $x = 5$ , under dark and (i)  $x = 5$ , under visible light.

**Table 3**  
Degradation percent of DBT under visible light and adsorption percent of DBT under dark in *n*-octane in the presence of Ni/CTM-41 and CTM-41 with different Si/Ti ratios.

Condition	Si/Ti	Sample	Percent of desulfurization (%)	
Visible light	50	CTMCM-41	68.60	
	50	Ni/CTMCM-41	93.50	
	10	CTMCM-41	74.90	
	10	Ni/CTMCM-41	94.50	
	7	CTMCM-41	86.20	
	7	Ni/CTMCM-41	96.00	
	5	CTMCM-41	95.60	
	5	Ni/CTMCM-41	98.60	
	Dark	50	CTMCM-41	44.70
		50	Ni/CTMCM-41	66.49
10		CTMCM-41	54.10	
10		Ni/CTMCM-41	73.19	
7		CTMCM-41	56.30	
7		Ni/CTMCM-41	81.34	
5		CTMCM-41	59.70	
5		Ni/CTMCM-41	83.15	

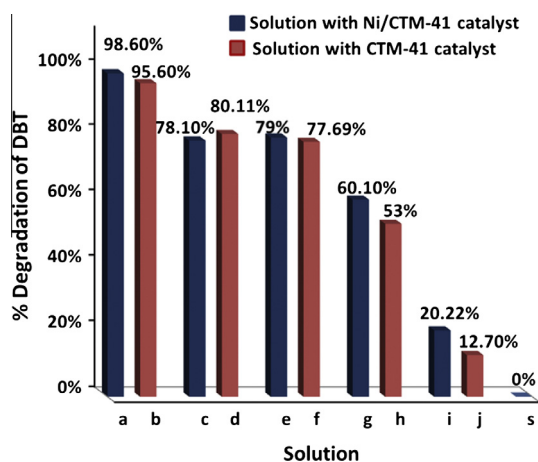


**Fig. 8.** Degradation percent of DBT in the presence of scavengers with Ni/CTM-41 (0.2) and CTM-41 (0.2). (a, b) without scavenger, (c, d)  $N_2$  added, (e, f) BQ added, (g, h) AO added and (i, j) DMSO added (s) standard solution.

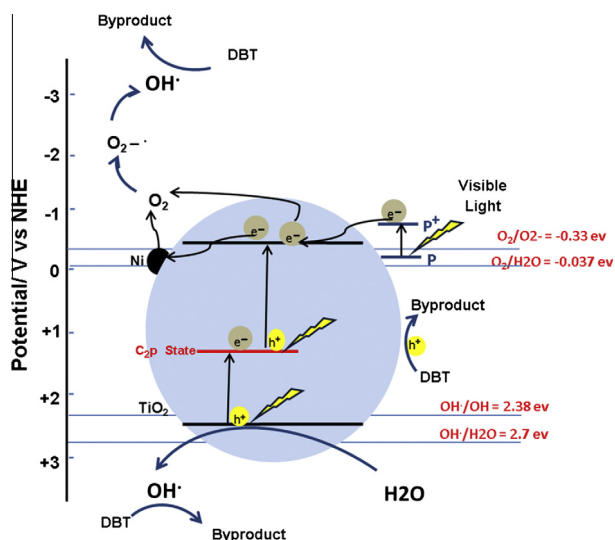


Fig. 9. Proposed mechanism for DBT degradation.

separated catalyst from previous step was added to alcohol and stirred at about 30 °C. After desorption, the solution was collected and analyzed by GC–MS analysis. The sulfur species were not observed on the GC chromatogram.

#### 4. Conclusions

In this work Ni/CTM-41 nanoparticles with various Si/Ti ratios (50, 10, 7, and 5) were prepared. The MCM-41 was used as a support and it was modified by titania, then Ni metal nanoparticles were deposited on titania by using the ultrasonic bath and PAD method. Characterization of Ni/CTM-41 revealed that Ni metal nanoparticles were distributed on the nanoporous molecular sieve support. Also, similar values band gaps of Ni/CTM-41 and CTM-41 proved that the nickel nanoparticles were dispersed on the surface. The Ni/CTM-41 samples had different UV–Vis absorption peaks in comparison with CTM-41. This was attributed to the interactions between the Ni nanoparticles and titania. The photocatalytic desulfurization of DBT was found strongly influenced by the amount of Ni atom presented on the catalyst. The Ni nanoparticles exhibited the photo desulfurization by providing a  $\pi$ -complexation adsorption. The results suggested that the photocatalytic desulfurization of DBT was highest when Ni/CTM-41 (Si/Ti = 5) was used as a catalyst. The results of GC–MS analysis also showed that the DBT was degraded by visible light irradiation under mild condition.

#### Acknowledgments

The support of Ferdowsi University of Mashhad (Research and Technology) is appreciated for the Project (3/19276, 17/10/2011). This work has also been supported by the “Iranian National Science Foundation: INSF” (No. 90001893).

#### Appendix A. Supplementary material

Supplementary data associated with this article can be found, in the online version, at <http://dx.doi.org/10.1016/j.jcis.2015.07.021>.

#### References

- [1] H. Li et al., *Green Chem.* 11 (6) (2009) 810–815.
- [2] Z. Juan et al., *Chem. Eng. J.* 156 (3) (2010) 528–531.
- [3] I.V. Babich, J.A. Moulijn, *Fuel* 82 (6) (2003) 607–631.
- [4] A.M. Dehkordi, Z. Kiaei, M.A. Sobati, *Fuel Process. Technol.* 90 (3) (2009) 435–445.
- [5] X. Li et al., *Appl. Catal. A* 254 (2) (2003) 319–326.
- [6] A. Samokhvalov et al., *Appl. Surf. Sci.* 256 (11) (2010) 3647–3652.
- [7] A. Samokhvalov et al., *Surf. Interface Anal.* 42 (9) (2010) 1476–1482.
- [8] C. Lanju, G. Shaohui, Z. Dishun, *Chin. J. Chem. Eng.* 15 (4) (2007) 520–523.
- [9] L. Cedeño-Caero et al., *Catal. Today* 172 (1) (2011) 189–194.
- [10] X. Si et al., *Catal. Lett.* 122 (3–4) (2008) 321–324.
- [11] R. Vargas, O. Núñez, *J. Mol. Catal. A: Chem.* 294 (1) (2008) 74–81.
- [12] P. Baeza et al., *Catal. Commun.* 9 (5) (2008) 751–755.
- [13] X. Ma et al., *Appl. Catal. B* 56 (1–2) (2005) 137–147.
- [14] R.T. Yang, A.J. Hernández-Maldonado, F.H. Yang, *Science* 301 (5629) (2003) 79–81.
- [15] A.J. Hernández-Maldonado, R.T. Yang, *Cataly. Rev.* 46 (2) (2004) 111–150.
- [16] M. Zarrabi, M.H. Entezari, E.K. Goharshadi, *RSC Adv.* 5 (44) (2015) 34652–34662.
- [17] A. Zach-Maor, R. Semiat, H. Shemer, *J. Colloid Interface Sci.* 357 (2) (2011) 440–446.
- [18] S. Zheng, L. Gao, *Mater. Chem. Phys.* 78 (2) (2003) 512–517.
- [19] J. Robertson, T.J. Bandosz, *J. Colloid Interface Sci.* 299 (1) (2006) 125–135.
- [20] K. Fuku et al., *J. Mater. Chem.* 22 (32) (2012) 16243–16247.
- [21] B.J. Aronson, C.F. Blanford, A. Stein, *Chem. Mater.* 9 (12) (1997) 2842–2851.
- [22] C. Galacho, M.M.L. RibeiroCarrott, P.J.M. Carrott, *Microporous Mesoporous Mater.* 100 (1–3) (2007) 312–321.
- [23] L. Marchese et al., *J. Phys. Chem. B* 101 (44) (1997) 8836–8838.
- [24] K.-E. Jeong et al., *J. Nanosci. Nanotechnol.* 10 (5) (2010) 3547–3550.
- [25] G. Mihai et al., *J. Porous Mater.* 16 (1) (2009) 109–118.
- [26] K. Mori et al., *Langmuir* 25 (18) (2009) 11180–11187.
- [27] H. Yang, Y. Deng, C. Du, *Colloids Surf., A* 339 (1) (2009) 111–117.
- [28] R. Chen et al., *Chin. J. Chem. Eng.* 14 (5) (2006) 665–669.
- [29] H.D.P. PrasetyoHermawan, J. IndrianaKartini, *Chem. Indo. J. Chem.* 2 (11) (2011) 135–139.
- [30] K.M. Reddy, S.V. Manorama, A.R. Reddy, *Mater. Chem. Phys.* 78 (1) (2003) 239–245.
- [31] A. Murphy, *Sol. Energy Mater. Sol. Cells* 91 (14) (2007) 1326–1337.
- [32] Y. Zhang, N. Zhang, Z.R. Tang, Y.J. Xu, *ACS Nano* 11 (6) (2012) 9777–9789.
- [33] F.T. Li, Y. Liu, Z.M. Sun, Y. Zhao, R.H. Liu, L.J. Chen, D.S. Zhao, *Catal. Sci. Technol.* 2 (2012) 1455–1462.